Supporting Information

Multifunctional Antifouling Sustainable Membranes Integrated MIL-125(Ti) and Carboxylated Cellulose Nanofibers for Self-Cleaning and Dye Degradation

Shuping Wu*, Lijuan Cui, Weijian Shi, Xiaokun Shi, Chao Xu

Institute of Polymer Materials, School of Materials Science & Engineering, Jiangsu University, Zhenjiang, Jiangsu Province, 212013, China

Experimental Section

Materials and chemicals

Polyvinylidene fluoride (PVDF), Polyvinylpyrrolidone (PVP, K30), *N*,*N*-Dimethylformamide（DMF），tetrabutyl titanate (TBT), methylene blue (MB), crystal violet (CV), malachite green (MG), Rhodamine B (RhB), congo red (CR), and methyl orange (MO) were purchased from Sinopharm Chemical Reagent Co., Ltd. *N*-methylpyrrolidone (NMP, 99.9%) and methanol (MeOH, GC, ⩾99.9%) were provided by Aladdin Reagent Co., Ltd. (Shanghai, China). Carboxylated cellulose nanofibers (CCNFs) and terephthalic acid (TPA) was purchased from China Maclean's Reagent Co.

Synthesis of MIL-125(Ti)

The synthesis of MIL-125(Ti) nanoparticles begins with the preparation of the precursor solution. Specifically, 1.8 g of TPA was dissolved in 40 mL of DMF and sonicated for 30 min to ensure complete dissolution, forming the organic ligand solution. Separately, 1 mL of TBT was dissolved in 6 mL of anhydrous methanol to create the titanium precursor solution, which is then mixed with the organic ligand solution and stirred at room temperature for 6 h to obtain a homogeneous mixture. The mixture was transferred to a stainless-steel autoclave lined with polytetrafluoroethylene and heated at 150 °C for 24 h to facilitate the solvothermal reaction, promoting MOF crystal formation. After the reaction, the autoclave is allowed to cool naturally to room temperature. The resulting product was collected by centrifugation at 9000 r/min for 8 min and washed three times with anhydrous methanol and DMF to remove unreacted precursors and byproducts. Finally, the centrifuged milky-while precipitate was dried at 70 °C for 12 h to obtain pure MIL-125(Ti) nanoparticles.

Preparation of PVDF/CCNF/MOF membrane

According to the specified mass ratios (Supporting information **Table S1**), PVDF, PVP, CCNF, and MIL-125(Ti) were mixed with the solvent NMP and sonicated for 1 h. The resulting mixture was stirred in a 70 °C water bath for 10 h and then left to degas for 12 h to obtain a homogeneous casting solution. This solution was poured onto a glass plate and spread using a coating bar at a speed of 5 mm/s. The glass plate was then immersed in deionized water to initiate phase separation, allowing the membrane to solidify. The separated membrane is submerged in deionized water for at least 12 h to remove residual solvents. Finally, the membrane was air-dried to obtain PVDF/CCNF/MIL-125(Ti) membranes, labeled as PCMT-1 to PCMT-5. PVDF/CCNF membranes without MIL-125(Ti), serving as experimental controls, were labeled as PCM-1 to PCM-4.

Characterization methods:

The structure and morphology of MIL-125(Ti) and the membranes were characterized using field emission scanning electron microscopy (FESEM, FEI NovaNano450) and transmission electron microscopy (TEM, JEOL JEM-2100 PLUS). The specific surface area, pore size distribution and adsorption-desorption characteristics of ZIF-8 crystals were determined using a fully automated specific surface area analyzer (BET, Micromeritics ASAP 2460). The structure of synthesized MIL-125(Ti) was identified by X-ray diffraction (XRD) using a BRUKER D8 ADVANCE with a diffraction range of 5-40° and a scanning speed of 7° (2θ) min^{-1}. Thermal stability of MIL-125(Ti) nanoparticles was analyzed by thermogravimetric analysis (TGA) using a HITACHI STA200, with a temperature range of 30-800°C and a heating rate of 20°C min^{-1}. Fourier-transform infrared spectroscopy (FTIR, Thermo Nicolet iS10) was employed to analyze the functional groups of MIL-125(Ti) and the membranes. The elemental composition of MIL-125(Ti) was identified using X-ray photoelectron spectroscopy (XPS, Thermo Escalab 250Xi). The surface morphology and roughness of

the membranes were evaluated by atomic force microscopy (AFM, Dimension Icon, Bruker, USA) over a scanning area of 8 μm × 8 μm. Static water contact angles (WCA) were observed at ambient temperature using an OCA15ec contact angle analyzer to characterize the hydrophilicity of the sample surfaces. Energy-dispersive X-ray spectroscopy (EDS, EDAX Octane Plus) was used to obtain elemental mapping of the membranes. The mechanical properties of the membrane samples were investigated using a universal testing machine (AGS-X, SHIMADZU), with all samples cut into 40 mm × 10 mm strips and subjected to a tensile test at a constant speed of 2 mm min^{-1} with a 10 N sensor. The zeta potential of the prepared membranes was measured using an electrokinetic analyzer (Nano Brook Omni, Brookhaven, USA) with pH adjusted from 3 to 11 using HCl (0.1 M) and KOH (0.1 M). Three different samples of each type were prepared and tested, with the mean values and standard deviations presented in the respective data sets.

Membrane separation tests:

The separation performance of PVDF/CCNF/MIL-125(Ti) membrane was evaluated using a combined circulating water vacuum pump and a sand core filtration unit. A 30 mg L^{-1} methylene blue (MB) solution served as the feed solution, with the feed concentration maintained constant throughout the separation test. Prior to the experiment, the membrane was compacted by filtering deionized water at 1 bar for 30 min to achieve a stable flux. Subsequently, pure water flux and separation experiments were conducted at 1 bar, respectively. The permeate flux (J, L m^{-2} h^{-1} bar^{-1}) was calculated according to equation (Eq.1).

$$J = \frac{V}{A \times \Delta t \times P} \qquad (1)$$

where V (L) is the permeate volume, A (m^2) is the effective membrane area, Δt (h) is the permeate time, and P is the operating pressure. The membrane rejection rate (R) is determined by Eq. 2:

$$R = \left(1 - \frac{C_p}{C_f}\right) \times 100\% \quad (2)$$

where C_p (mg L^{-1}) and C_f (mg L^{-1}) are the permeate and feed solution concentrations, respectively. The concentration of dye solution before and after filtration was determined using a UV-visible spectrophotometer (UV, Shimadzu UV-2700).

Membrane self-cleaning and dye degradation test

The self-cleaning and dye degradation of the PVDF/CCNF/MIL-125(Ti) membrane was performed under UV irradiation. A MB solution with a concentration of 30 mg L^{-1} was prepared as the feed solution. The initial concentration of the MB solution was measured using a UV-Vis spectrophotometer at the characteristic wavelength of 664 nm. The membrane samples were compacted by filtering deionized water at 1 bar for 30 min to achieve a stable flux, and the initial pure water flux (J_0) was recorded. The membrane was then placed in a filtration device, and the permeation flux (J_1) was measured after filtration. The fouled membrane was subjected to UV irradiation for 4 h. After irradiation, the membrane was thoroughly rinsed with deionized water to remove loose contaminants. The pure water flux of the cleaned membrane (J_2) was measured at 1 bar. The MB concentration in the solution before and after irradiation was measured to evaluate the degradation efficiency. The flux recovery ratio (FRR), total fouling ratio (R_t), reversible flux decline ratio (R_r), and irreversible fouling ratio (R_{ir}) were calculated using Eqs. 3-6.

$$FRR = \frac{J_2}{J_0} \times 100\% \quad (3)$$

$$R_t = \left(\frac{J_0 - J_1}{J_0}\right) \times 100\% \quad (4)$$

$$R_r = \left(\frac{J_2 - J_1}{J_0}\right) \times 100\% \quad (5)$$

$$R_{ir} = \left(\frac{J_0 - J_2}{J_0}\right) \times 100\% \qquad (6)$$

Table.S1 The ingredients of PVDF/CCNF/MOF membrane.

Membrane ID	PVDF (g)	PVP (g)	NMP (g)	CCNF (g)	MIL-125(Ti) (g)
PCM-1	1.5	0.05	8.35	0.1	0
PCM-2	1.5	0.05	8.25	0.2	0
PCM-3	1.5	0.05	8.15	0.3	0
PCM-4	1.5	0.05	8.05	0.4	0
PCMT-1	1.5	0.05	8.05	0.4	0.2
PCMT-2	1.5	0.05	8.05	0.4	0.4
PCMT-3	1.5	0.05	8.05	0.4	0.6
PCMT-4	1.5	0.05	8.05	0.4	0.8
PCMT-5	1.5	0.05	8.05	0.4	1.0

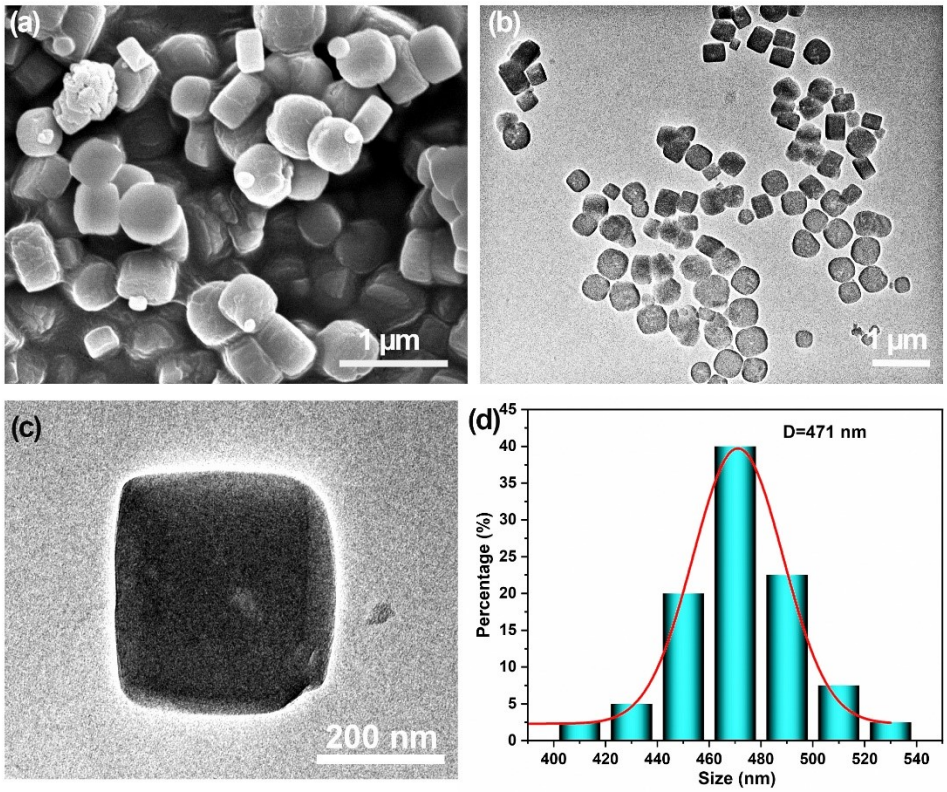

Fig. S1. Microstructure and size distribution of MIL-125(Ti) nanoparticles. (a) SEM image; (b) TEM image; (c) Single MIL-125(Ti)'s morphology; (d) Size distribution histogram.

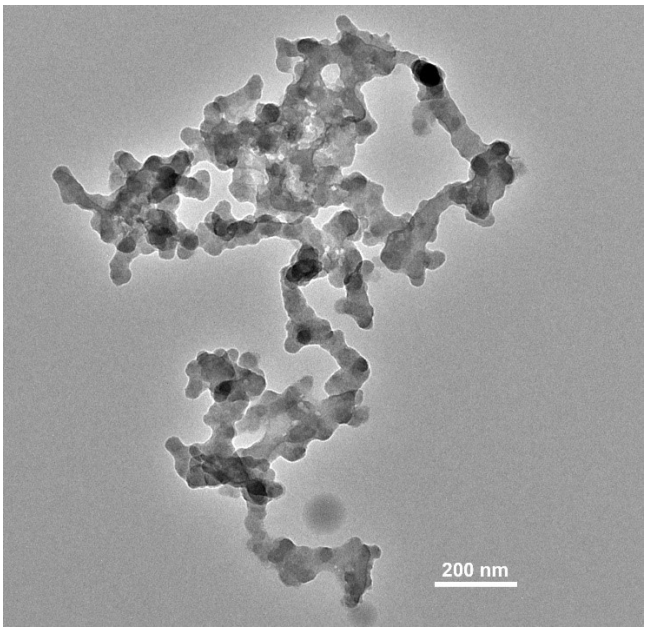

Fig. S2. TEM image of CCNF.

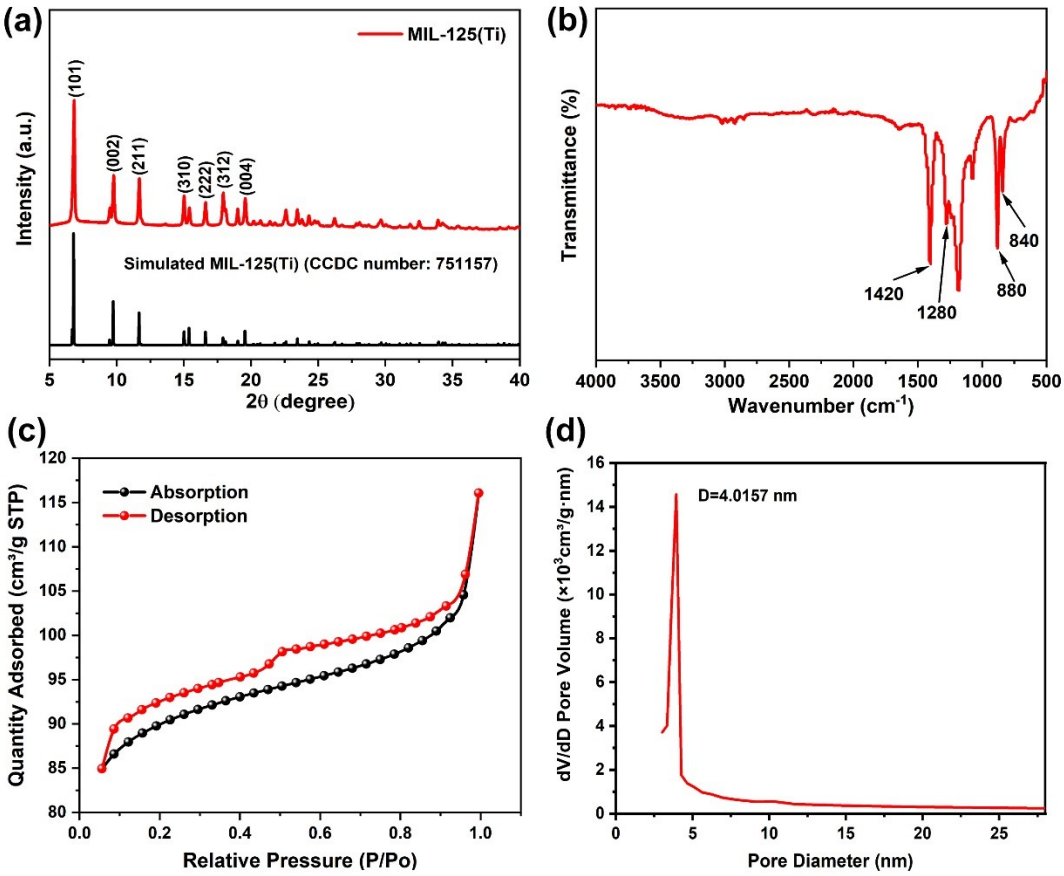

Fig. S3. Structural and pore analysis of MIL-125(Ti). (a) XRD: the red curve represents the diffraction peaks of the experimentally synthesized MIL-125(Ti), while the black curve represents the simulated MIL-125(Ti) (CCDC number: 751517) diffraction peaks. (b) FTIR. (c) Nitrogen adsorption-desorption isotherms. (d) Pore size distribution, with MIL-125(Ti) pore size primarily centered around 4 nm.

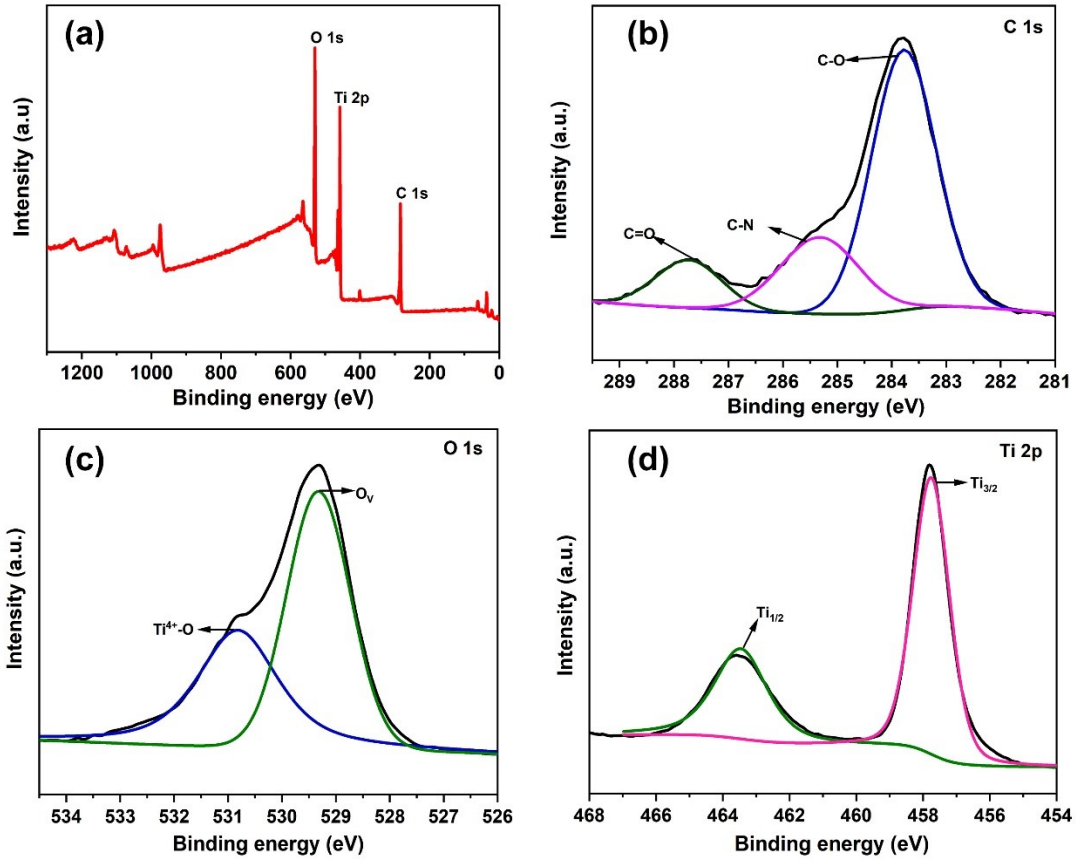

Fig. S4. XPS spectra of MIL-125(Ti). (a) The whole spectrum. (b) C 1s. (c) O 1s. (d) Ti 2p.

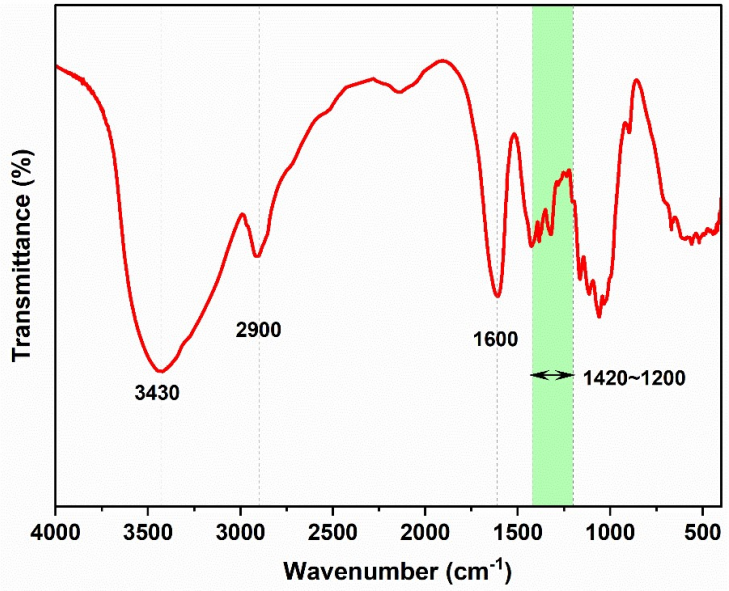

Fig. S5. FTIR of CCNF.

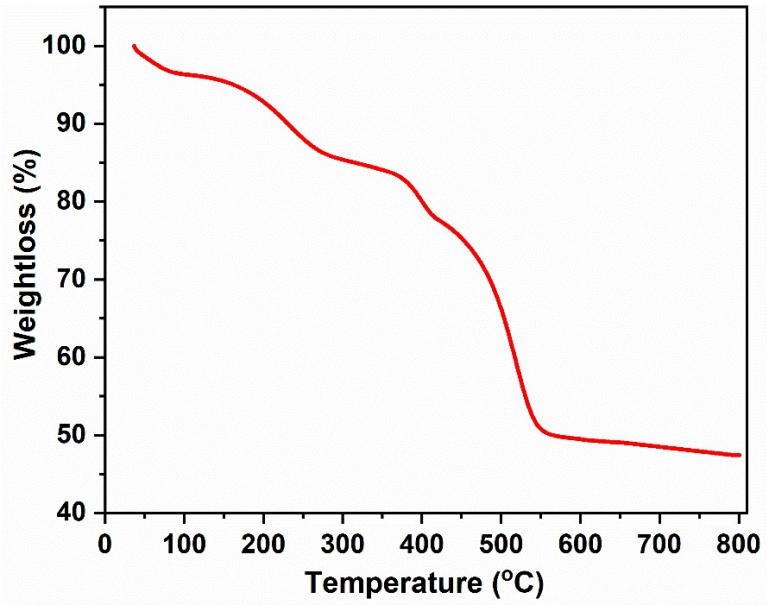

Fig. S6. TGA curve of MIL-125(Ti).

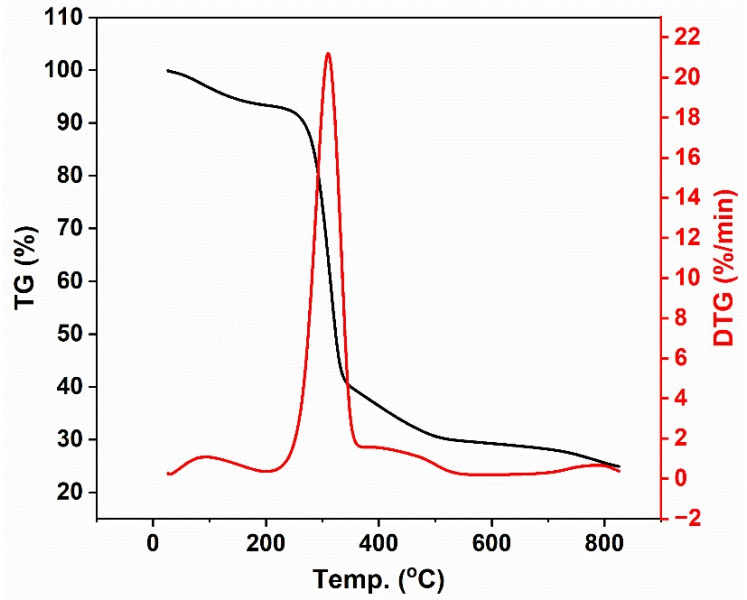

Fig. S7. Thermal stability of CCNF.

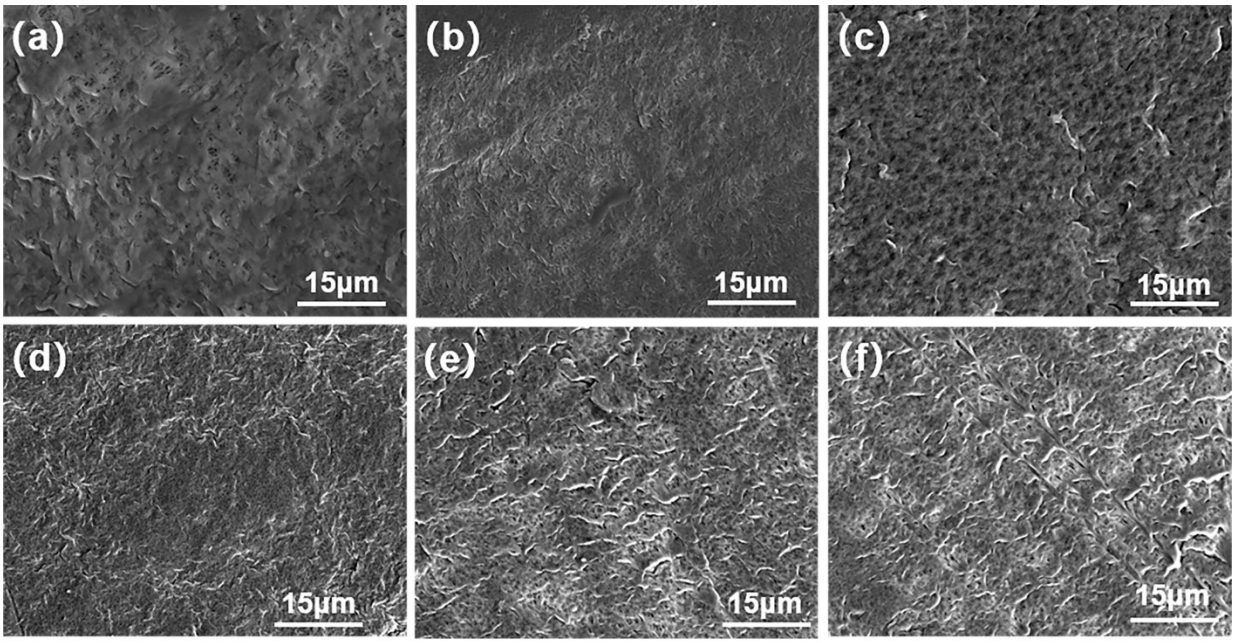

Fig. S8. Surface morphology of the PVDF/CCNF/MOF membranes with different MIL-125(Ti) loadings. (a) PCM-4; (b) PCMT-1; (c) PCMT-2; (d) PCMT-3; (e) PCMT-4; (f) PCMT-5.

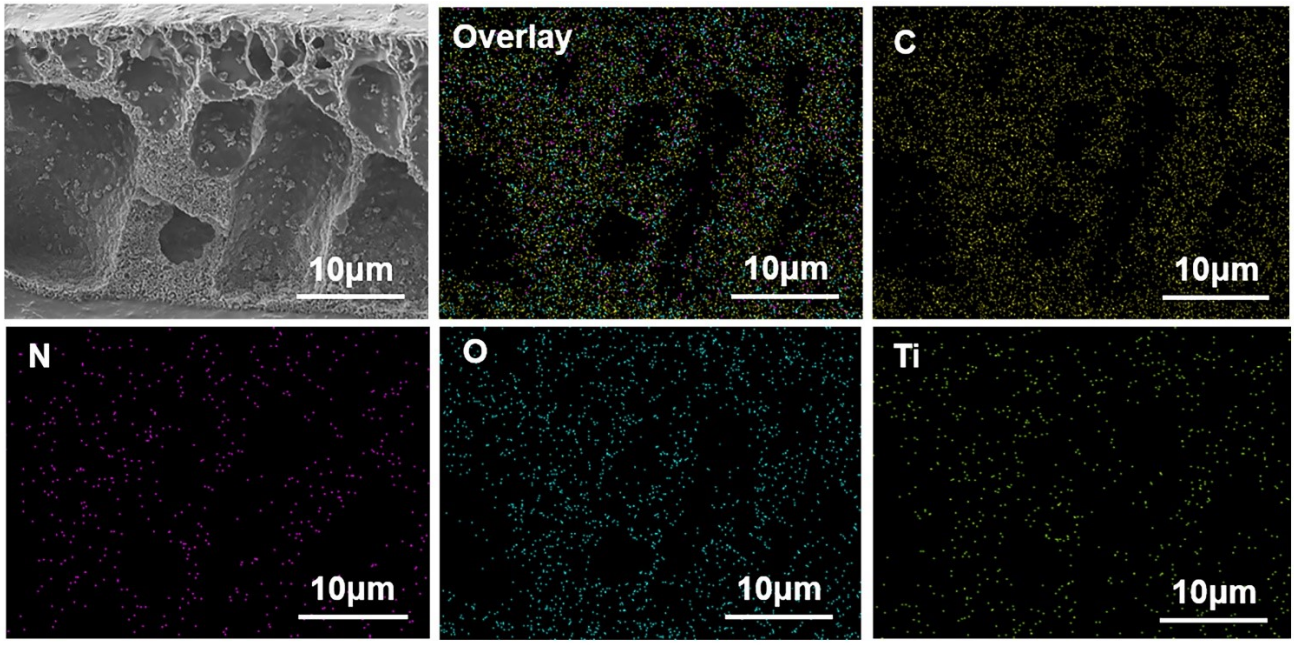

Fig. S9. Cross-sectional morphology of the PVDF/CCNF/MOF membrane.

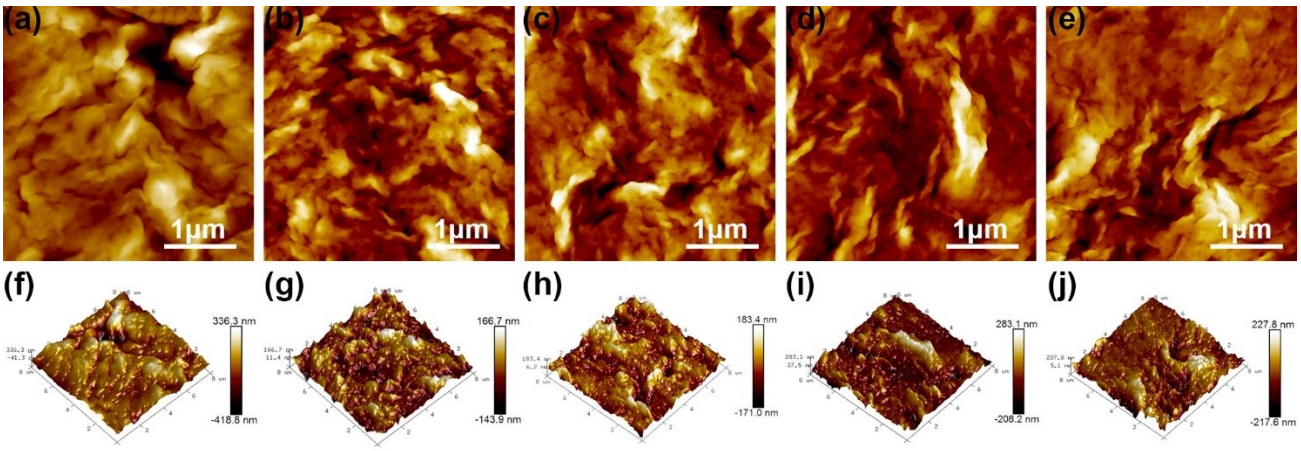

Fig. S10. 2D and 3D AFM images of the PVDF/CCNF/MIL-125(Ti) membrane series. (a, f) PCMT-1, exhibiting the lowest surface roughness, -184.3 nm~165.2 nm, with a relatively flat surface. (b, g) PCMT-2, with a roughness range of -143.9 nm~166.7 nm, showing more surface fluctuations on the surface. (c, h) PCMT-3, where the surface becomes rougher with increased roughness from -171.0 nm to 183.4 nm and a noticeable increase in particle density. (d, i) PCMT-4, further increasing in surface roughness to a range of -208.2 nm to 283.1 nm, displaying more complex topographical features. (e, j) PCMT-5, although the roughness slightly decreases, it remains within -217.6 nm to 227.8 nm, indicating surface heterogeneity caused by the high content of MIL-125(Ti).

Table.S2 Surface roughness of PVDF/CCNF/MOF membranes with different MIL-125(Ti) loadings.

Membrane ID	**PCMT-1**	**PCMT-2**	**PCMT-3**	**PCMT-4**	**PCMT-5**
Root mean square roughness (Rq, nm)	43.1	47.3	55.7	62.8	91.8
Roughness average (Ra, nm)	33.5	36.4	41.2	46.7	67.9

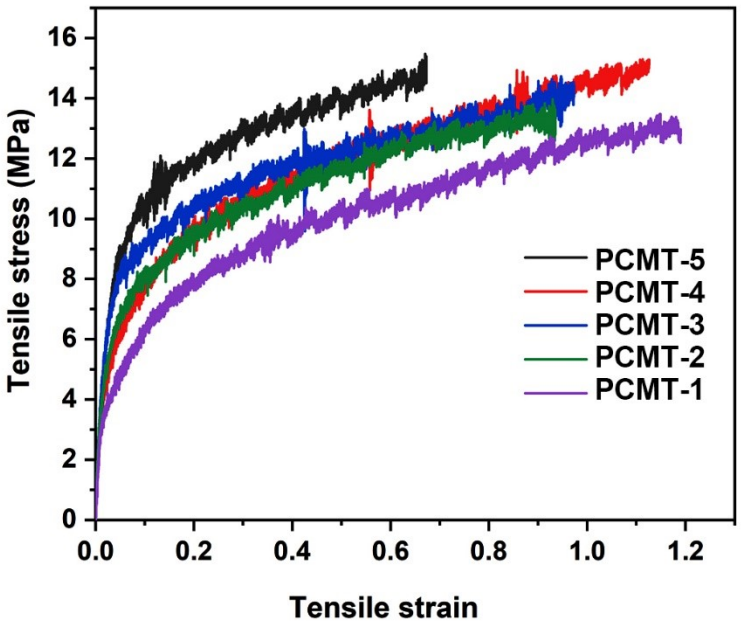

Fig. S11.The tensile stress-strain curves of PVDF/CCNF/MOF membranes

Table.S3 Tensile strength and Elongation at Break of PVDF/CCNF/MOF membranes.

	PCMT-1	PCMT-2	PCMT-3	PCMT-4	PCMT-5
Tensile strength (TS, MPa)	12.96	13.43	14.43	15.27	15.38
Elongation at Break (EB, %)	119	93.5	97.3	121.6	67.2

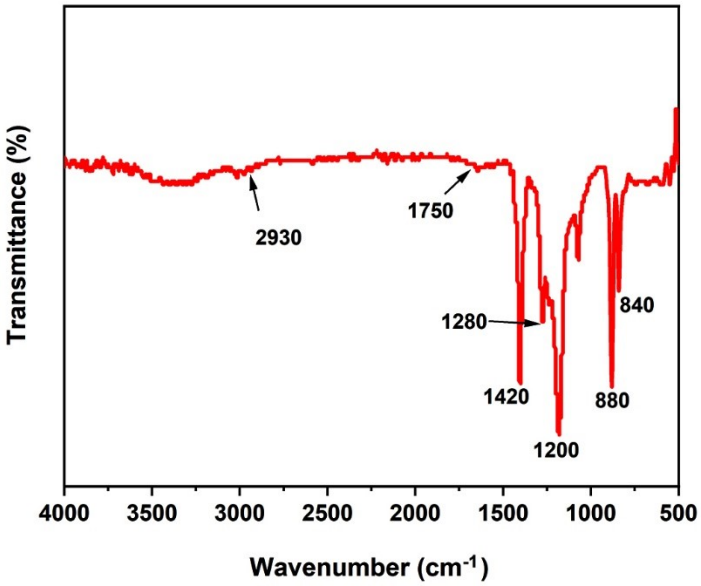

Fig. S12. FTIR spectrum of PCMT-4

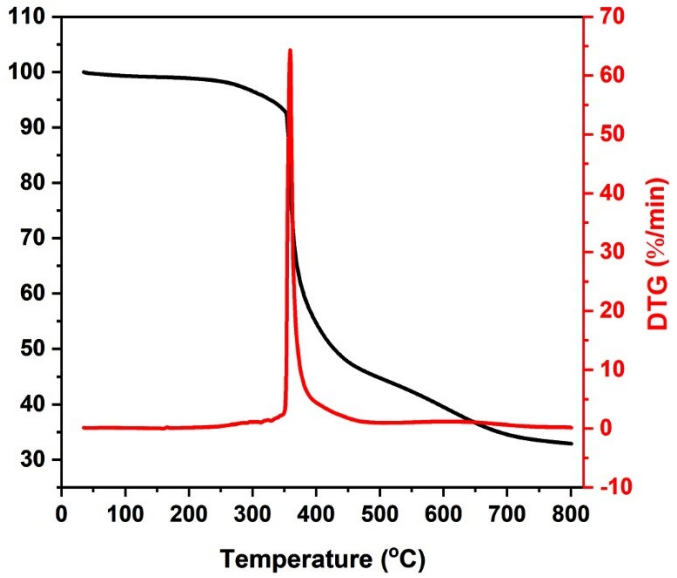

Fig. S13. Thermal stability of PCMT-4

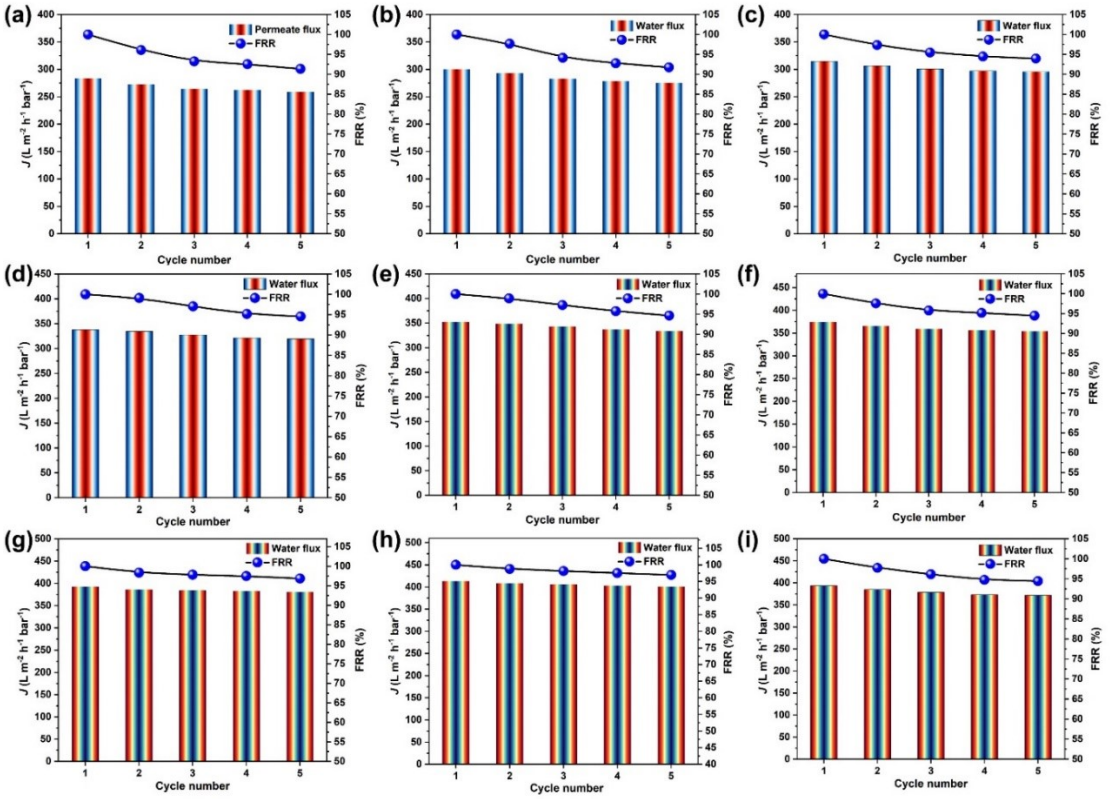

Fig. S14. Changes in pure water permeability (*J*) and flux recovery ratio (*FRR*) of different types of PVDF/CCNF/MIL-125(Ti) membranes over five cycles. (a) PCM-1; (b) PCM-2; (c) PCM-3; (d) PCM-4; (e) PCMT-1; (f) PCMT-2; (g) PCMT-3; (h) PCMT-4; (i) PCMT-5.

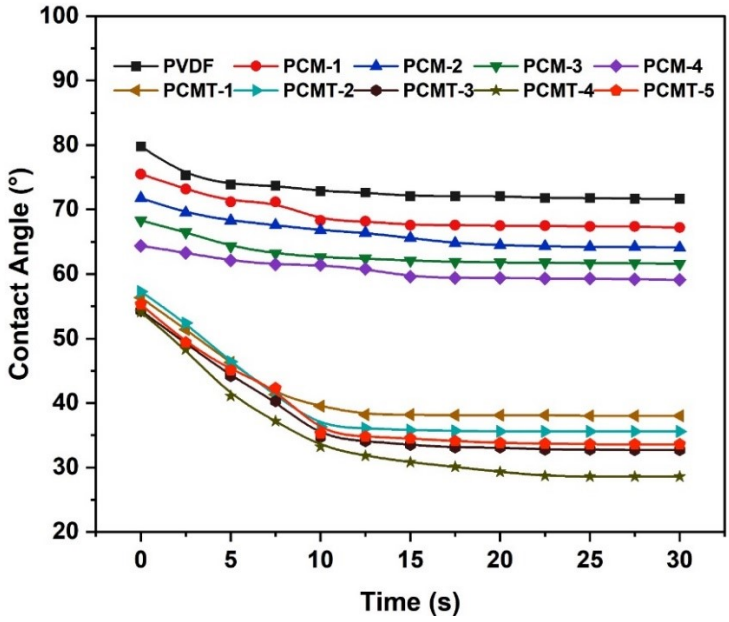

Fig. S15. Time-dependent contact angle of different types of PVDF/CCNF/MIL-125(Ti) membranes.

Table.S4 Comparative performance of photocatalytic membranes for dye removal

Photocatalytic membrane	Target dye	Removal efficiency	FRR (%)	Reference
PVDF/CCNF/MIL-125(Ti) (this work)	MB, CV, MG, RhB	98.9%, 99.3%, 97.5%, 94.8%	94	This work
g-C_3N_4@MXene/PES	CR, TB, TC	98%, 96%, 86%	n/a	1
N-$Bi_2O_2CO_3$@MXene	CR, TB, RhB	99.9%, 73.4%, 46.7%	n/a	2
PES/GO@TiO_2	MB	95.1%	86.1%	3
NCQDs-TiO_2/PAA/PES	MB	94.9%	83.9%	4
TiO_2/PVDF	CR, RY145	67%, 77%	n/a	5
Ti_3C_2/WO_3/PVDF	RhB	n/a	94%	6
PVDF/BiOBr	RhB, TC, Cr^{6+}	100%, 93.8%, 74.6%,	n/a	7
MIL-53(Fe)/PVDF	TC	87%	n/a	8
TiO_2/Al_2O_3	Direct Black168	70%	n/a	9
$ZnIn_2S_4$	Fluvastatin	97.19%	76.58%	10

*Trypan blue (TB), tetracycline (TC), polyethersulfone (PES), polydopamine (PDA), polyethyleneamine (PEI), polyethersulfone (PES), graphene oxide (GO), nitrogen doped carbon quantum dots modified TiO2 (NCQDs-TiO2), polyacrylic acid (PAA), Reactive Yellow 145 (RY 145).

Table.S5 Selective dye removal performance of PCMT-4 membranes (30 mg·L^{-1} dye solution, 1 bar pressure, UV irradiation for 4 h).

Dye type	Dye name	Charge	Removal efficiency (%)
Cationic	CV	+	99.3
Cationic	MB	+	98.9
Cationic	MG	+	97.5
Cationic	RhB	+	94.8
Anionic	CR	–	82.1
Anionic	MO	–	79.4

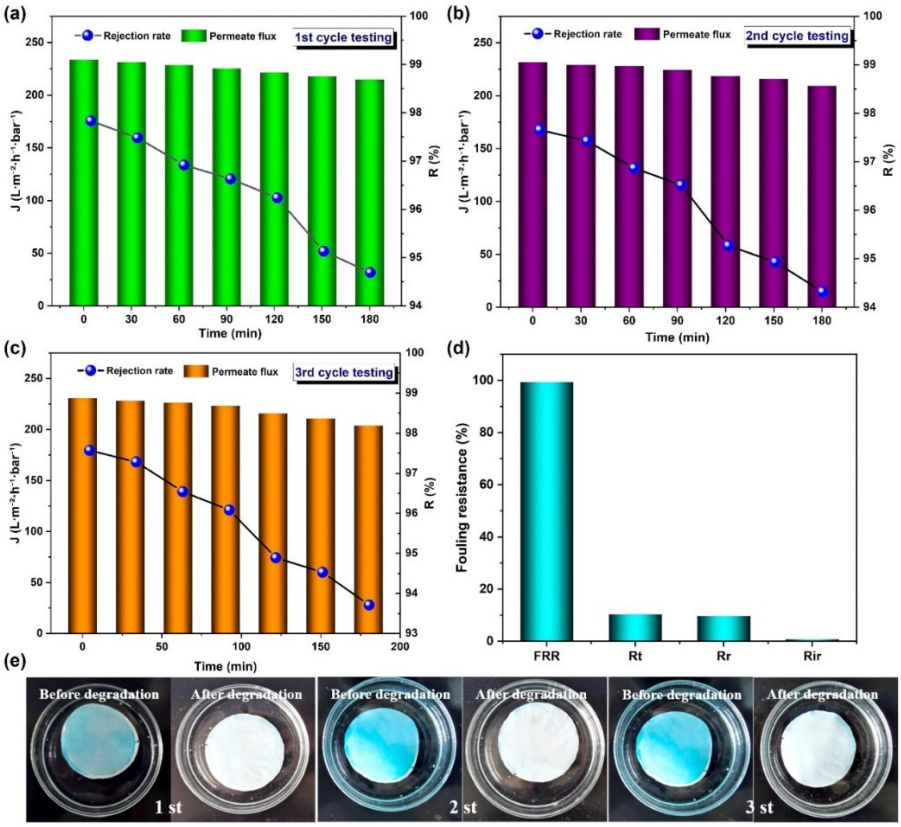

Fig. S16. Recyclability (a-c), antifouling abilities (d), and self-cleaning performance (e) of the PVDF/CCNF/MIL-125(Ti) membranes.

Notes and references

1. G. Zeng, Z. He, T. Wan, T. Wang, Z. Yang, Y. Liu, Q. Lin, Y. Wang, A. Sengupta and S. Pu, *Separation and Purification Technology*, 2022, **292**, 121037.
2. Q. Lin, G. Zeng, G. Yan, J. Luo, X. Cheng, Z. Zhao and H. Li, *Chemical Engineering Journal*, 2022, **427**, 131668.
3. C. Ding, X. Qin, Y. Tian and B. Cheng, *Journal of Membrane Science*, 2022, **659**, 120789.
4. Z. W. Heng, W. C. Chong, Y. L. Pang, L. C. Sim and C. H. Koo, *Journal of Environmental Chemical Engineering*, 2021, **9**, 105388.
5. E. Erusappan, S. Thiripuranthagan, R. Radhakrishnan, M. Durai, S. Kumaravel, T. Vembuli and N. J. Kaleekkal, *Journal of Environmental Chemical Engineering*, 2021, **9**, 105776.
6. X. Pang, S. Xue, T. Zhou, Q. Xu and W. Lei, *Ceramics International*, 2022, **48**, 3659-3668.
7. F. Bi, Z. Zheng, R. Li, R. Du, L. Zhao, S. Xiao, L. Wang and X. Dong, *Chemical Engineering Journal*, 2025, **507**, 160781.
8. C.-J. Wu, I. Valerie Maggay, C.-H. Chiang, W. Chen, Y. Chang, C. Hu and A. Venault, *Chemical Engineering Journal*, 2023, **451**, 138990.
9. H. Zhang, X. Quan, S. Chen, H. Zhao and Y. Zhao, *Separation and Purification Technology*, 2006, **50**, 147-155.
10. T. Liu, L. Wang, X. Liu, C. Sun, Y. Lv, R. Miao and X. Wang, *Chemical Engineering Journal*, 2020, **379**, 122379.